WindSat Passive Microwave Polarimetric Signatures of the Greenland Ice Sheet

Li Li, *Senior Member, IEEE*, Peter Gaiser, *Senior Member, IEEE*, Mary R. Albert, David G. Long, *Fellow, IEEE*, and Elizabeth M. Twarog

***Abstract*—WindSat has systematically collected the first global fully polarimetric passive microwave data over both land and ocean. As the first spaceborne polarimetric microwave radiometer, it was designed to measure ocean surface wind speed and direction by including the third and fourth Stokes parameters, which are mostly related to the asymmetric structures of the ocean surface roughness. Although designed for wind vector retrieval, WindSat data are also collected over land and ice, and this new data has revealed, for the first time, significant land signals in the third and fourth Stokes parameter channels, particularly over Greenland and the Antarctic ice sheets. The third and fourth Stokes parameters show well-defined large azimuth modulations that appear to be correlated with geophysical variations, particularly snow structure, melting, and metamorphism, and have distinct seasonal variation. The polarimetric signatures are relatively weak in the summer and are strongest around spring. This corresponds well with the formation and erosion of the sastrugi in the dry snow zone and snowmelt in the soaked zone. In this paper, we present the full polarimetric signatures obtained from WindSat over Greenland, and use a simple empirical observation model to quantify the azimuthal variations of the signatures in space and time.**

***Index Terms*—Greenland ice sheet, ice, polarimetric microwave radiometry, snow, WindSat.**

I. Introduction

FOR DECADES, microwave radiometry has proven to be a valuable tool for polar research because of its high sensitivity to the physical properties of snow. For example, microwave emission is very sensitive to snow wetness; hence, Abdalati and Steffen [1] and Mote and Anderson [27] used microwave data to detect snowmelt over Greenland. Over dry snow regions, snow and surface air temperatures have been inferred from satellite radiometer data [32], [37], [42]. Grody and Basist [18] and West *et al.* [45] also showed that snow stratification can change microwave emission and its frequency dependence. Abdalati and Steffen [2] and Flach *et al.* [12] modeled the relationship between microwave emission and snow accumulation/microstructure. The influence of hoar formation on the emission was also demonstrated using ground and satellite-based data [19], [25]. Shuman *et al.* [31] demonstrated how to detect the formation of hoar with passive microwave data, creating a reliable dating tool for snow pits and ice cores, therefore improving the interpretation of ice core paleoclimatic records. Recent studies also revealed correlations between azimuthal modulation of microwave emission from the Special Sensor Microwave/Imagers (SSM/I) and snow surface roughness induced by winds [24].

The aforementioned work used heritage satellite microwave radiometers, such as the SSM/I and the Advanced Microwave Scanning Radiometer (AMSR), which measure only vertically and horizontally polarized radiation. These two polarizations represent the first two of the four elements of the radiometric Stokes vector, which fully defines electromagnetic radiation. The third and fourth components of the Stokes vector, representing the cross correlation of the first two components, were originally neglected because they were presumed to be too small or zero at satellite footprint scales [38], [40]. However, several airborne radiometer campaigns over the ocean demonstrated measurable ($\sim$2.5 K maximum) third and fourth Stokes parameters with signatures that are mostly related to the asymmetric structures of the ocean surface roughness [15], [30], [48]. Following this discovery, the U.S. Naval Research Laboratory (NRL) developed and launched WindSat, the first spaceborne polarimetric microwave radiometer, under the sponsorship of the U.S. Navy and the National Polar-orbiting Operational Environmental Satellite System [14]. Using the polarimetric signature over the ocean, WindSat has demonstrated that it is indeed feasible to retrieve ocean surface vector winds from a multifrequency polarimetric radiometer (e.g., [9]).

In addition to successfully retrieving ocean vector winds and supporting new science in oceanography, the WindSat mission has measured unexpected and unexplained polarimetric signals (the third and fourth Stokes parameters) from Greenland and Antarctica that are about eight times stronger than those from the ocean. For example, Fig. 1 depicts all four modified Stokes parameters collected from ascending and descending passes at 18.7 GHz over the Northern Hemisphere for the period of February 1–9, 2004. The strong third and fourth Stokes parameters stand out clearly and uniquely over Greenland against a much weaker ocean and land background. Although the third Stokes parameter shows a small ($<$ 1 K) signal over land elsewhere, over Greenland the third Stokes parameter varies between -10 to 20 K, which is roughly eight times stronger than the ocean polarimetric signal.

In this paper, we focus our analysis on WindSat data over Greenland, characterizing its polarimetric signatures and their associated temporal and spatial variations. We also discuss the related surface and volume scattering theory related to these observed signatures. The main purpose of this paper is to present the unique polarimetric signatures of polar ice sheets uncovered

Manuscript received February 23, 2007; revised September 4, 2007. This work was supported in part by the Office of Naval Research and in part by the NPOESS Integrated Program Office.

L. Li, P. Gaiser, and E. M. Twarog are with the Naval Research Laboratory, Washington, DC 20375 USA.

M. R. Albert is with Cold Regions Research and Engineering Laboratory, Hanover, NH 03755 USA.

D. G. Long is with the Center for Remote Sensing, Microwave Earth Remote Sensing Laboratory, Brigham Young University, Provo, UT 84602 USA.

Digital Object Identifier 10.1109/TGRS.2008.917727

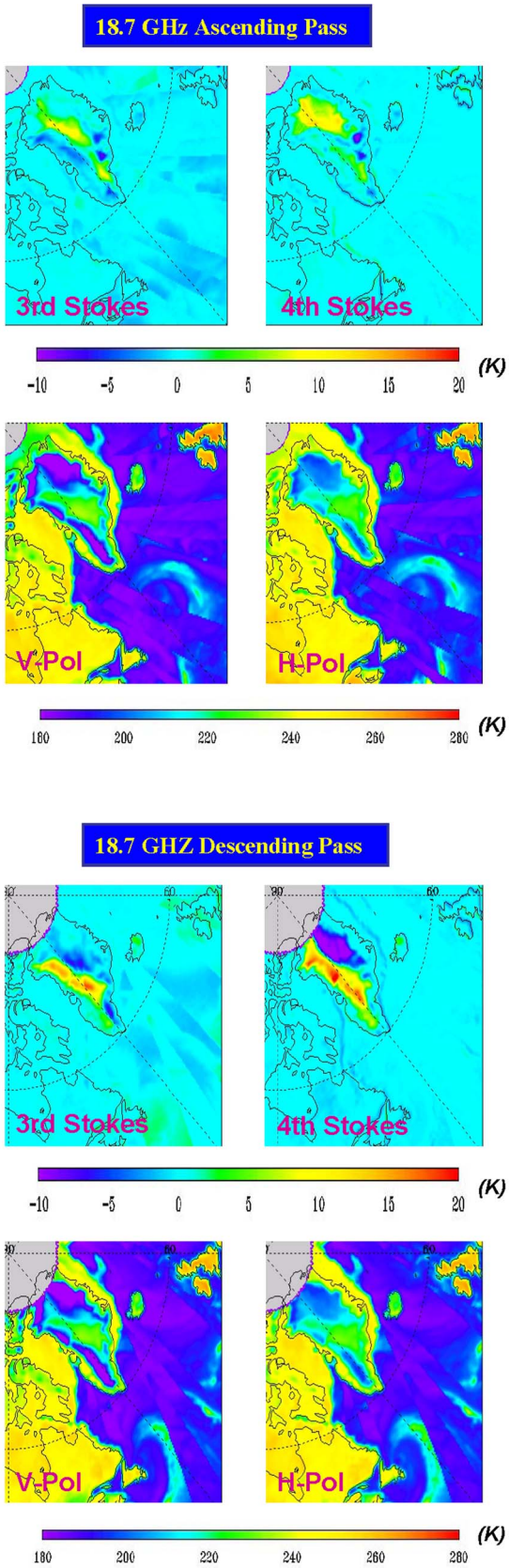

Fig. 1. Composite WindSat polarimetric measurements at 18.7 GHz for the four Stokes parameters collected by WindSat during February 1–10, 2003.

by WindSat and to stimulate new polar research activities in areas of snow asymmetry structure and its interaction with microwaves.

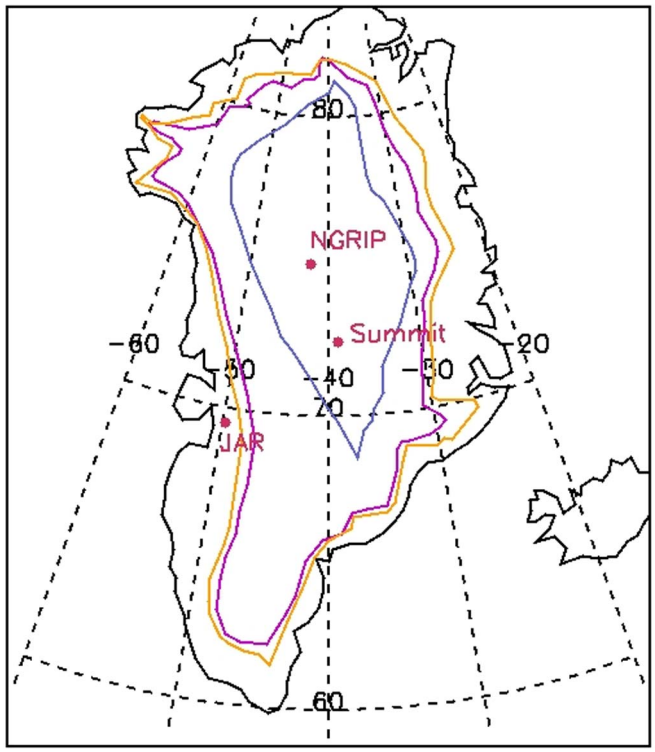

Fig. 2. Greenland map showing postulated locations of key ice facies [10] and study site locations for WindSat data.

II. Greenland Climatology

As one of Earth's two great ice sheets, the Greenland ice sheet is an environmentally sensitive area that plays a significant role in global sea level and climate change. The polar firn contains records of both long- and short-term local climate through the layering of the firn that is created by patterns of snow deposition and of hoar complex formation. The firn physical properties control microwave emission, linking the sensor data to environmental change in the polar region. The physical properties of the snow and firn also control air–snow exchange processes, which affect both the atmospheric chemistry (e.g., [11]) and the chemical and physical content of the firn that eventually becomes the ice core record (e.g., [4]). Therefore, understanding the polarimetric signature, uniquely afforded by WindSat, and its relationship to the snow properties and microstructures could have a profound impact on climate studies.

Based on snow metamorphism and melt, the Greenland ice sheet can be subdivided into several distinct facies or zones [10], [23]. These zones are shown in Fig. 2 and are defined as follows. The dry-snow zone of the central Greenland, delineated by the blue line in Fig. 2, experiences negligible snow melt due to its high altitude and low physical temperature. Nevertheless, snowpack diagenesis does take place, resulting in growth in snow grain size and formation of a winter wind slab. The annual accumulation in the dry snow zone is closely related to precipitation and/or wind flow patterns. Down-slope from the dry snow zone is the percolation zone where summer melt water percolates down through the snowpack. In Fig. 2, the percolation zone is depicted by the purple line. The melting and refreezing cycle produces larger snow grains, ice lenses, pipes, and layering. Further down-slope in the soaked or wet-snow

zone delineated by the orange line, melt water saturated the snowpack down to the previous summer surface. Such wet snow in the summer generates thick layers of dense ice during the refreezing in the fall. As a general rule, there is no significant melting in the winter anywhere in Greenland.

The glacier exhibits a large range of surface roughness in various forms, such as sastrugi, which are indicators of air–snow interaction and often can be detected by many high-resolution remote-sensing sensors. Herzfeld [20] performed ice surface classification based on image data such as synthetic aperture radar. Germain *et al.* [15] and Nolin and Payne [29] extracted surface roughness from the Multi-angle Imaging SpectroRadiometer (MISR) data. These data can be potentially useful in interpreting rough surface effect on WindSat polarimetric signatures.

The Greenland Climate Network (GC-Net) collects climate information on Greenland's ice sheet using automatic weather stations (AWSs) [33]. Among them, we selected three station locations in two different ice sheet zones, as shown in Fig. 2. The Summit and North Greenland Ice-Core Project (NGRIP) sites are both well studied and located inside the dry snow zone, but have different snow characteristics. The JAR site is within the soaked snow zone. These sites have very different seasonal atmospheric temperature variations and different snow properties that reflect changes in surface energy balance, as described above, which result in significantly different emission/scattering signatures in WindSat data.

III. WindSat Instrument and Data

The modified Stokes vector provides a full characterization of electromagnetic radiation [38]. It is defined as

$$I_{\mathrm{S}} = \begin{bmatrix} T_{\mathrm{V}} \\ T_{\mathrm{H}} \\ U \\ V \end{bmatrix} = C \begin{bmatrix} \frac{1}{\eta}\langle E_{\mathrm{V}} E_{\mathrm{V}}^{*} \rangle \\ \frac{1}{\eta}\langle E_{\mathrm{H}} E_{\mathrm{H}}^{*} \rangle \\ \frac{2}{\eta}\mathrm{Re}\langle E_{\mathrm{V}} E_{\mathrm{H}}^{*} \rangle \\ \frac{2}{\eta}\mathrm{Im}\langle E_{\mathrm{V}} E_{\mathrm{H}}^{*} \rangle \end{bmatrix} \tag{1}$$

where the first two Stokes parameters T_{V} and T_{H} are the brightness temperatures of vertical and horizontal polarizations, respectively. The third (U) and fourth (V) Stokes parameters represent the cross-correlational terms of vertical and horizontal polarizations. The total radiated energy is represented by $I = T_{\mathrm{V}} + T_{\mathrm{H}}$, while the linear polarization difference $Q = T_{\mathrm{V}} - T_{\mathrm{H}}$, together with U and V, describes fully the polarized components. In the past, Q was often referred as polarization difference and used extensive to represent polarized nature of natural radiation. U and V were generally assumed to be zero and neglected in microwave radiometry [38], [40]. For decades, satellite microwave radiometers, including SMMR, SSM/I, and AMSR-E, have been measuring the first two components for many science applications, neglecting the third and fourth components.

As a fully polarimetric microwave radiometer, WindSat measures all four parameters of the modified Stokes vector at 10.7, 18.7, and 37.0 GHz, along with T_{V} and T_{H} at 6.8 and 23.8 GHz. The conically scanned WindSat has a forward swath of about 1000 km and a 53° Earth incidence angle (EIA). The 830-km orbit is sun synchronous with ascending equatorial crossings at 6:00 P.M. local time.

In the standard WindSat Sensor Data Record (SDR) products, all the brightness temperatures of different frequencies are resampled and beam-averaged to a common spatial resolution of approximately 40 km by 60 km (the approximate 6-GHz ground footprint). We then bin the SDR swath data onto the 25-km Northern and Southern Hemispheres EASE-grid and compile them into separate daily ascending and descending data files. A time series of brightness temperature data are then extracted from the EASE-Grid data for the selected Greenland sites. In this paper, we use two years of WindSat data from February 2003 to January 2005.

IV. Azimuthal Modulation Modeling

A random medium is reflection symmetric if, for any realization of the medium permittivity and permeability, there is another realization that is a mirror image to the former realization. For example, a wind roughened ocean surface can be regarded as reflection symmetric with respect to the wind direction. In general, the signatures of the U and V are directly related to the reflection symmetry of the target media. Using a reflection operator for Maxwell's equations, Yueh *et al.* [47] showed that, if a random medium is reflection symmetric about an azimuthal plane, T_{V} and T_{H} are even (i.e., cosine) functions of azimuthal direction, while U and V are odd (i.e., sine) functions. For a random medium with no preferred azimuthal orientation, the reflection symmetry holds for any azimuthal plane. In this case, the U and V can be shown to be zero. U and V respond most strongly to the azimuthal asymmetry structure of the snowpack and, thus, are strong functions of the observation geometry. T_{V} and T_{H} respond mostly to the dielectric properties and temperature of the snow/firn. When analyzing U and V, it is essential to account for the azimuth modulations to separate the observation geometry effects from environmental variations. Then, we can examine the changes in the microwave signature to infer the temporal and spatial variations in the physical properties of the ice sheet. A simple and effective way to define the microwave signature is to construct an empirical observation model with a small number of model parameters that can account for the signature variability and separate different effects in the measurements.

Given the constant EIA of the WindSat conical scanning geometry, U and V over Greenland are functions of satellite azimuth look angle (observation geometry) and ice-sheet characteristics [5]. We thus adopt the following simple empirical observation model for the polarimetric emissions:

$$\begin{bmatrix} U \\ V \end{bmatrix} = \begin{bmatrix} U_0 + U_1 \sin(\phi - \phi_1) + U_2 \sin 2(\phi - \phi_2) \\ V_0 + V_1 \sin(\varphi - \varphi_1) + V_2 \sin 2(\varphi - \varphi_2) \end{bmatrix} \tag{2}$$

where ϕ is the compass azimuth observation angle at the pierce point ($\phi = 0^\circ$ points to the north, $\phi = 90^\circ$ points to the east); $\{Ui\}$ and $\{Vi\}$ are the coefficients of the azimuth modulation, and $\{\phi_i\}$ and $\{\varphi_i\}$ are the orientations of different harmonics. The first harmonic coefficients U_1 and V_1 describe the emission signatures that are related to the 180° asymmetry structures of the snowpack. The second harmonic coefficients U_2 and V_2 represent the 90° asymmetry structures. For the more familiar case of ocean surface scattering, the 180° asymmetry is induced by the asymmetric surface features on the leeward and windward faces of large-scale waves, while the 90° asymmetry

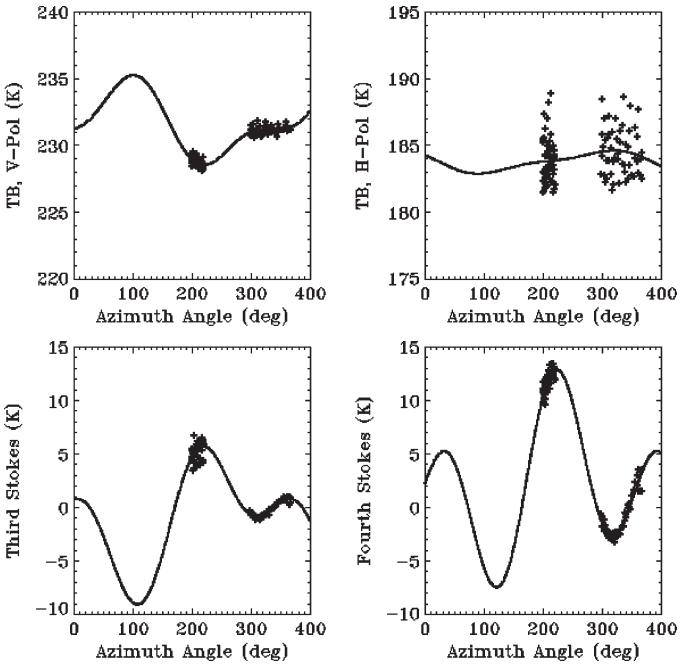

Fig. 3. Four Stokes parameters at 10.7 GHz observed by WindSat over the Summit study site in Greenland during April 2003. The solid line is the fitted second-order harmonic model. See text for discussion.

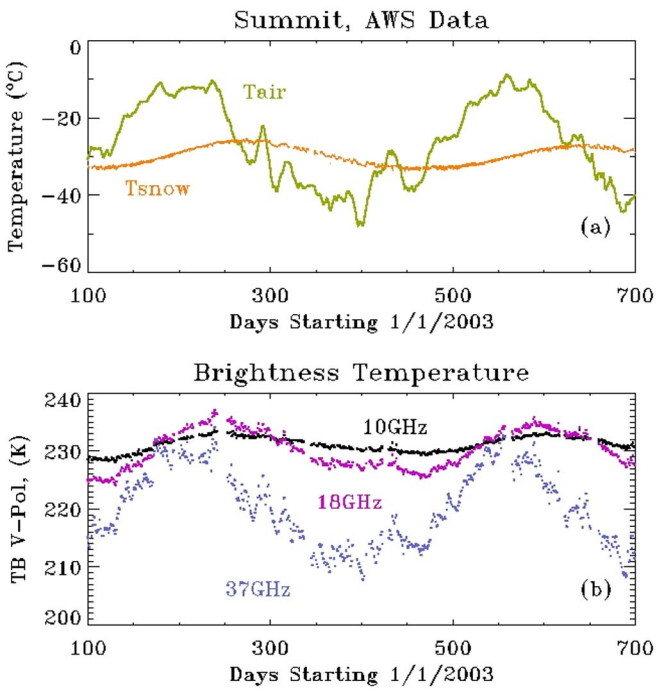

Fig. 4. Time series of WindSat observations over the Greenland Summit study site from April 1, 2003 to December 30, 2004. The 10.7-, 18.7-, and 37.0-GHz data are color coded with black, purple, and blue, respectively. (a) *In situ* air and snow temperature. A 30-day running average is applied to the air temperature to delineate its trend and minimize short-term diurnal and storm fluctuations. (b) Vertically polarized brightness temperature of descending orbits.

is due to the difference in surface roughness between upwind and crosswind directions. For the case of firn, combined surface roughness and volume scattering from snow dunes and sastrugi can produce similar 180° and 90° asymmetry structures [24].

Our approach is to examine the temporal variations of the model coefficients (2) of WindSat polarimetric data at different locations in Greenland. Signatures in vertical and horizontal polarization channels, as well as AWS *in situ* data, are included for comparison to illustrate the new information content in the polarimetric channels. Because the dry snow zone characteristics change slowly over Greenland, we estimate the model parameters using a 30-day time window and intervals. Measurements from both ascending and descending passes are combined in the estimations. For wet snow zone, the melt signal is very strong and rapid, and it dominates the data point before the onset of the melt. Thus, our observation data model can still capture the dynamics of the polarimetric signature well on monthly time scales, although the model error will increase slightly.

V. Results

A. Azimuthal Modulation Over Dry-Snow Zone

Scatter plots of 10.7-GHz brightness temperatures versus azimuth look angles are shown in Fig. 3 for the month of April 2003. The azimuthal angle is defined as the compass azimuth angle of the radiometer antenna beam at the pierce point of the Earth's surface. The measurements are extracted from the WindSat EASE-Grid data set near the Summit site. Each data point represents a single satellite overpass with no binning or averaging performed in the azimuthal direction. The measurements centered on 210° correspond to satellite descending passes at approximately 7:30 A.M. local time; while the measurements around 340° are from ascending passes near 4:30 P.M. local time.

The top left panel in Fig. 3 shows 10.7-GHz vertical polarization brightness temperatures. There is an asymmetric brightness temperature difference of about 2 K between ascending and descending passes with less than 1 K of scatter in the data. This 2 K difference is not likely a diurnal effect because 10.7-GHz radiation has a snow penetration depth of more than 10 m, while the hourly sampled snow temperature varies very slowly with time, even at 1-m depth [as shown in Fig. 4(a)]. We note that in the horizontal polarization plotted in the top right panel, scatter in the data are large, more than 8 K, which overwhelms any similar small azimuthal modulations on the order of 1–2 K. The large scatter in horizontal brightness temperatures and the relatively small dynamic range in vertical polarization are consistent with previous theoretical and experimental studies [13], [31].

In sharp contrast to T_{V} and T_{H}, the bottom panels showing 10.7 GHz U and V observations reveal well-pronounced azimuthal dependencies, both within and between the passes. The scatter in the data are much less than T_{H} and comparable to the scatter in T_{V}. However, there are clearly azimuthal dependencies within the 290° to 360° azimuth angles of ascending passes, while T_{V} shows azimuthal dependencies only between ascending and descending passes. The peak-to-peak signals of the azimuthal modulations are also much larger, about 7 and 18 K for U and V, respectively. This is a unique and extremely strong signal compared to either the ocean or other land areas. Although the azimuth sampling range is limited, the data fit the empirical second-order harmonic model in (2) very well, as depicted by the solid lines. We also fit the model to WindSat U and V data from different months and obtained similar azimuthal modulation signals, indicating that WindSat

polarimetric data can be well modeled using the second-order harmonic model.

In addition to the strong azimuthal signal, a striking signature of the Greenland polar firn is its stronger V signals relative to U. Fig. 1 shows that such a signature exists for most part of Greenland. This unique signature has never been observed in nature before and cannot be explained by surface scattering alone. Tsang [39] formulated a theory for passive microwave polarimetry for the case of discrete scatterers and rough surface scattering. Using vector radiative transfer simulations, he showed that U and V can be very significant if the discrete scatterers have certain statistical asymmetrical configurations. He also suggested it is possible to retrieve information concerning particle orientation distribution from the U and V. Following these studies, polarimetric signatures of 1-D rough soil surfaces and 2-D asymmetrical surfaces were also investigated using an integral equation approach [22], [43]. In addition, fully polarimetric two-scale models were developed for ocean surface scattering and compared with experiment data (e.g., [15], [48], and [49]). Except for the volume scattering model developed by [39], all ocean and land surface scattering models predicted a much weaker fourth Stokes parameter. Exploring this strong polarimetric signature could potentially open a new area of microwave remote sensing of the cryosphere.

B. Temporal Variation of Dry-Snow Zone

1) Summit Site: Fig. 4(a) plots time series of *in situ* air temperature at 1-m height and snow temperature at 1-m depth extracted from the GC-Net AWS stations at the Summit site. A 30-day running average is applied to the air temperature to delineate its trend and minimize short-term diurnal and storm fluctuations. Note that no running average was applied to snow temperature at 1-m depth, since it shows very little fluctuation and minimal temporal or seasonal variation. At this site, snow accumulation events occur throughout the year. The total accumulation is about 65 cm/year.

In the dry snow region of Greenland, T_{V} and T_{H} are very sensitive to the effective physical temperature of the dry firn [37], [50]. Fig. 4(b) shows time series of WindSat vertically polarized brightness temperatures over the Summit site for the 10.7-, 18.7-, and 37-GHz channels. Clearly, the WindSat measurements follow the general seasonal variations of *in situ* air or snow physical temperatures, although the different frequencies peak at different times. For example, the 10.7-GHz data peak about early September (Day 245 and 600), while the 18-GHz data peak about five days earlier than 10-GHz data. This phase difference between the two peaks is due to the different penetration depths at the different frequencies [37]. In summer, there is a temperature gradient in the snow due to the warming of near-surface layers, while the deeper layers are still cold from the previous winter. The 37-GHz brightness temperatures respond more closely to the air temperature due to its shallower penetration depth whereas because of its greater penetration depth, the 10.7-GHz data correspond more closely to the snow temperature at depth. For example, there is no clear summer maximum from June to August (days 150 to 220) for air temperature, but there are two local maximums at days 175 and 240. A more distinct structure is the short-term air temperature increase around day 290. All of these air temperature variation features are evident in the 37-GHz data but are not reproduced in the 10.7- and 18.7-GHz data, which are more correlated with deeper snow temperatures.

Fig. 5(a)–(d) shows time series of WindSat first (U_1 and V_1) and second (U_2 and V_2)-order harmonic coefficients of (2) at the Summit study site. Each coefficient data point is derived using a 30-day time window, as discussed in Section IV. The U and V harmonics at 10.7-, 18.7-, and 37-GHz channels are included and color-coded in the plots. Overall, the harmonic coefficients of both U and V can reach as high as 10 K individually, or 20 K for combined first and second harmonics, which is the total signal measured by radiometer and is very large compared to the azimuthal variations observed over the ocean. Well-pronounced seasonal variations are evident in most harmonic coefficients, except for the second harmonic of the U in Fig. 5(c). For all three frequencies, the V signals are about the same strength as the U over Greenland. As discussed earlier, this is in striking contrast to a weaker V signatures generated by ocean surface scattering. In general, all harmonic coefficients increase starting early winter and peak in spring or early summer, and remain close to their minimums during summer and fall. The first harmonics peak near mid-April [Fig. 5(a)] and early June [Fig. 5(b)] for U and the V, respectively, which suggests that 180° asymmetry snow structures affect the U and V differently. Similarly for V, there is an offset between the second peak in Fig. 5(b) (around day 530, as indicated by line A) for the first harmonic, and in Fig. 5(d) (about day 470, as indicated by line B) for the second harmonic. This suggests that the 180° and 90° asymmetrical structures change differently to impact the fourth Stokes parameter.

The seasonal variations demonstrated in Fig. 5 reflect changes in snow characteristics. The significant impacts of the surface roughness on the first two modified Stokes parameters have been well studied in the past. Therefore, it is important to understand the surface roughness effects on the third and fourth Stokes parameters. Albert and Hawley [3] analyzed surface roughness data collected at the centimeter-to-meter scale during the winter-over experiment in 1998 at Summit, Greenland. They found that the change in surface roughness is related to the winter formation and summer erosion of sastrugi, which are the most visible asymmetrical features over polar firn. The snow accumulates through episodic snowfall events, and the wind subsequently erodes it into rough features and sastrugi during times of high winds and cold temperatures. The dune crests are oriented orthogonally to the wind direction, while the sastrugi are oriented parallel to the wind direction. They become more level during the summer by sublimation and deflation [16], [17]. Albert and Hawley [3] showed that surface roughness heights are less than 8 cm from late June to later December but started to increase around January. From January to March, the surface roughness became up to 25 cm. Such a temporal signature in the surface roughness is very consistent with seasonal variations of harmonic coefficients in Fig. 5, as discussed in previous paragraph. However, it is necessary to point out that such a consistency does not suggest that surface scattering by sastrugi is the mechanism that produces the strong polarimetric signatures. Numerical simulations of ocean [49] and snow [46] surfaces all indicate that rough surface scattering alone cannot produce large polarimetric signature, particularly the fourth Stokes parameter. Although rigorous theoretical and experimental studies are needed to determine the exact physics

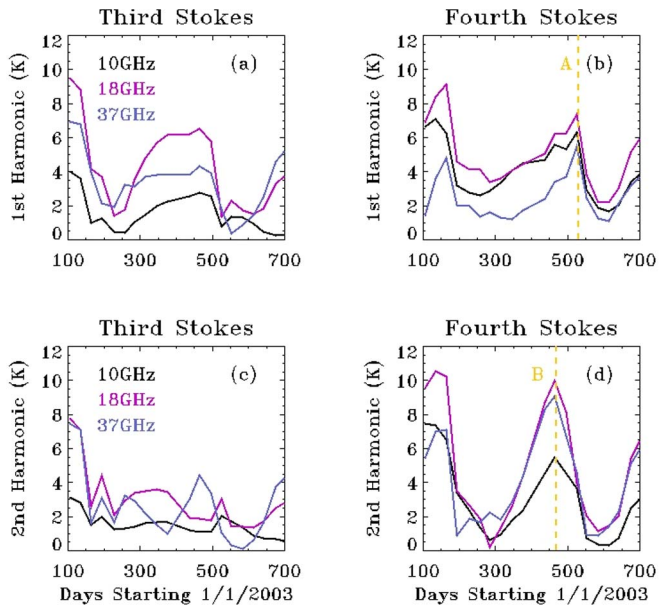

Fig. 5. Time series of WindSat observations over the Greenland Summit study site from April 1, 2003 to December 30, 2004. The 10.7-, 18.7-, and 37.0-GHz data are color coded with black, purple, and blue, respectively. (a) First harmonic of U. (b) First harmonic of V. (c) Second harmonic of U. (d) Second harmonic of V.

behind the observation, it is possible that the WindSat U and V data respond to the coupled volume and surface scattering associated with asymmetry structures of polar firn microstructure and rough surfaces.

In addition to their sensitivity to snowpack temperatures, brightness temperatures also depend on the snow microstructure (grain size, shape, and arrangement and nature of bonds), accumulation, stratification, and surface roughness. For example, Fig. 6 plots time series of the ratio of vertical and horizontal polarized brightness temperatures (termed the $T_{\mathrm{V}}/T_{\mathrm{H}}$ ratio), which is much less sensitive to physical temperature variations than brightness temperatures themselves but still has significant variations on both weekly and seasonal time scales that are not correlated with temperature variations. The modified Q $(T_{\mathrm{V}} - T_{\mathrm{H}})$ is also plotted in Fig. 6 for comparison and shows similar structures. There are sustained progressive declines of the $T_{\mathrm{V}}/T_{\mathrm{H}}$ ratio from April to mid-July 2003 (day 100 to 200, as indicated by label "A"), and from February to mid-May 2004 (day 400 to 500, as indicated by label "B"). The $T_{\mathrm{V}}/T_{\mathrm{H}}$ ratio rises subsequently outside these two declining periods. Using observations from the Greenland Ice Sheet Project II site, [31] attributed the summertime decreases in SSM/I 37 GHz $T_{\mathrm{V}}/T_{\mathrm{H}}$ ratio to the decreases in near surface density and increases in centimeter-scale surface roughness, which are created by intense insolation and periodic surface temperature change that cause the formation of coarse-grained summertime hoar complex. Such conclusion should apply to WindSat data also, since WindSat was built on SSM/I heritage and nearly the same center frequency and incidence angle for the 37-GHz channels [14]. Additional discuss on the summertime variation in $T_{\mathrm{V}}/T_{\mathrm{H}}$ for firn are contained in [26].

Similar to the $T_{\mathrm{V}}/T_{\mathrm{H}}$ ratio, the U and V signals are expected to be much less sensitive to snow temperatures than to microstructures of snow. If we refer to the variation of the signal strength or sensitivity with frequency as the "spectral

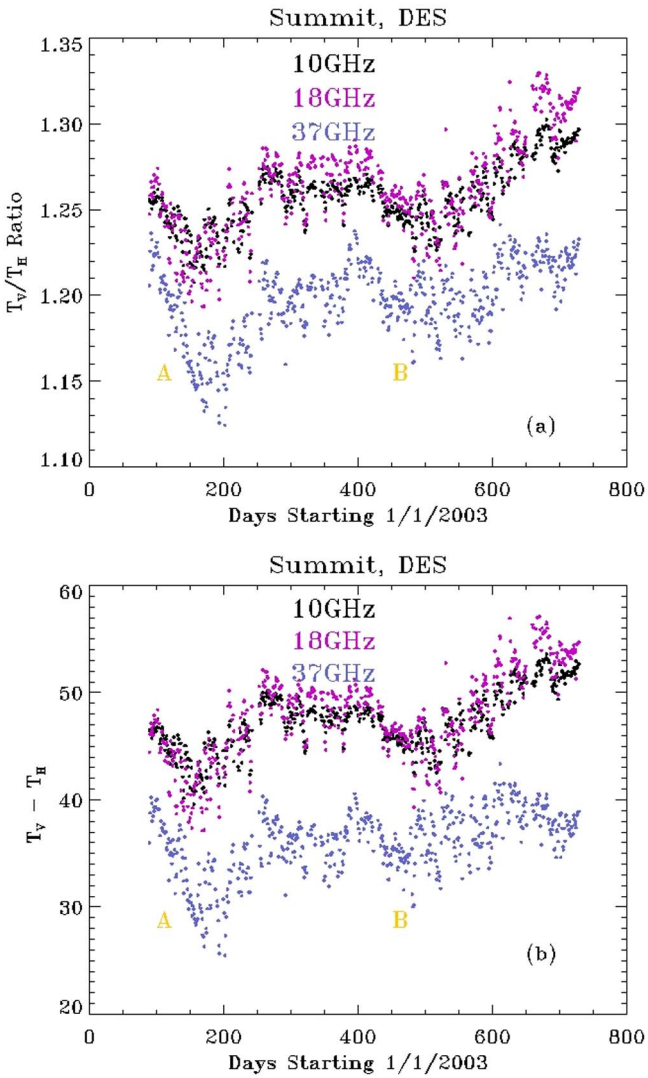

Fig. 6. Time series of WindSat $T_{\mathrm{V}}/T_{\mathrm{H}}$ ratio of descending orbits observations over the Greenland Summit study site from April 1, 2003 to December 30, 2004. The 10.7-, 18.7-, and 37.0-GHz data are color coded with black, purple, and blue, respectively.

signature," the U and V show very different spectral signatures than the $T_{\mathrm{V}}/T_{\mathrm{H}}$ ratio. For example, Fig. 6 shows that $T_{\mathrm{V}}/T_{\mathrm{H}}$ ratios of the lower frequencies at 10.7 and 18.7 GHz are stronger than the ratio at 37 GHz; while Fig. 5(d) shows that the 18.7- and 37-GHz channels fourth Stokes parameter second harmonics are stronger than at 10 GHz. The second harmonic of the third Stokes parameter shows lower sensitivity to frequency than any of the other harmonics. These differences between the $T_{\mathrm{V}}/T_{\mathrm{H}}$ ratios and polarimetric channels, along with their differences in seasonal variations represent new information available from polarimetric passive microwave data. They can also serve as additional validation to theoretical models, which now must be consistent with not only T_{V} and T_{H}, but also U and V. Although the $T_{\mathrm{V}}/T_{\mathrm{H}}$ ratio has been used effectively to identify hoar formation events in summertime, it does not provide sufficient constraints to differentiate snow parameters, and therefore, no accurate model has yet been developed to quantitatively estimate hoar amount and snow accumulation [2]. Inclusion of the polarimetric observations can provide the additional constraints to help separate snow parameters.

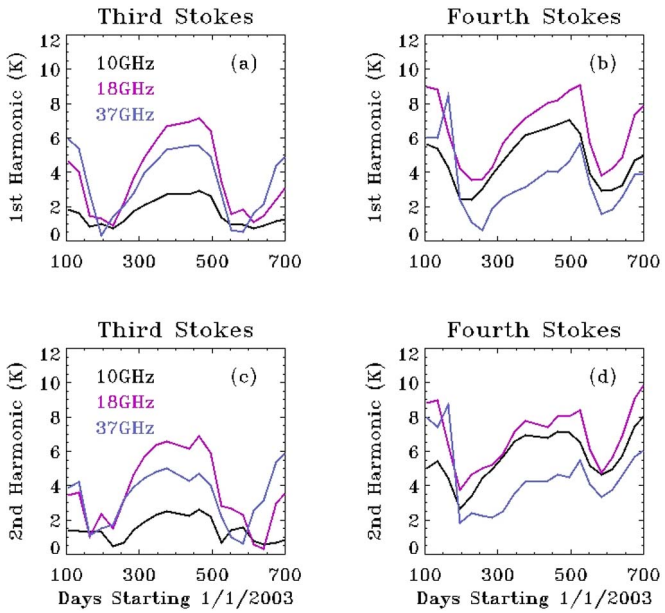

Fig. 7. Time series of WindSat observations over NGRIP site from April 1, 2003 to December 30, 2004. The 10.7-, 18.7-, and 37.0-GHz data are color coded with black, purple, and blue, respectively. (a) First harmonic of U. (b) First harmonic of V. (c) Second harmonic of U. (d) Second harmonic of V.

Another way to examine the new information content is to compare the spatial distribution of the first two modified Stokes parameters against the third and fourth Stokes parameters. Fig. 1 shows that the spatial patterns of U and V are very different from T_{V} and T_{H}. In contrast, T_{V} and T_{H} have very similar patterns and are highly correlated. In other words, there is significant decorrelation or new information content in the polarimetric channels.

2) NGRIP Site: It is necessary to test the repeatability and examine the spatial variations of WindSat polarimetric signature in the dry-snow zone. Moving downslope to the northeast region of the dry-snow zone at the NGRIP site as shown in Fig. 2, the snow accumulation is about 40 cm/year. While the Summit and NGRIP sites are separated by only about 300 m in elevation, the NGRIP climatological summer air temperatures are a few degrees warmer than at the Summit, which leads to relatively larger mean snow grain size [23]. Long and Drinkwater [23] analyzed Seasat-A scatterometer data over the Greenland and showed that the volume scattering is significantly stronger in the northeast region (covering the NGRIP site) than at the Summit. Therefore, it is reasonable to expect differences in WindSat data between these two sites.

Fig. 7 provides charts similar to Fig. 5 but at the NGRIP site. All Stokes parameters have similar seasonal variations as at the Summit site, but there are indeed significant differences in the spectral signatures from these two sites. Again, the U signals are relatively weak during the summer and stronger in late winter and early spring, which is similar to the polarimetric signatures at the Summit in Fig. 5. However, the V signals are strong during all seasons except summer. The V signal at the NGRIP site is even stronger than the U, but is comparable to the V signal at the Summit. The second harmonic of U has a stronger signal and a distinct seasonal variation at NGRIP [Fig. 7(c)], while it is relatively small and flat at the Summit [Fig. 5(c)]. In addition, frequency dependencies

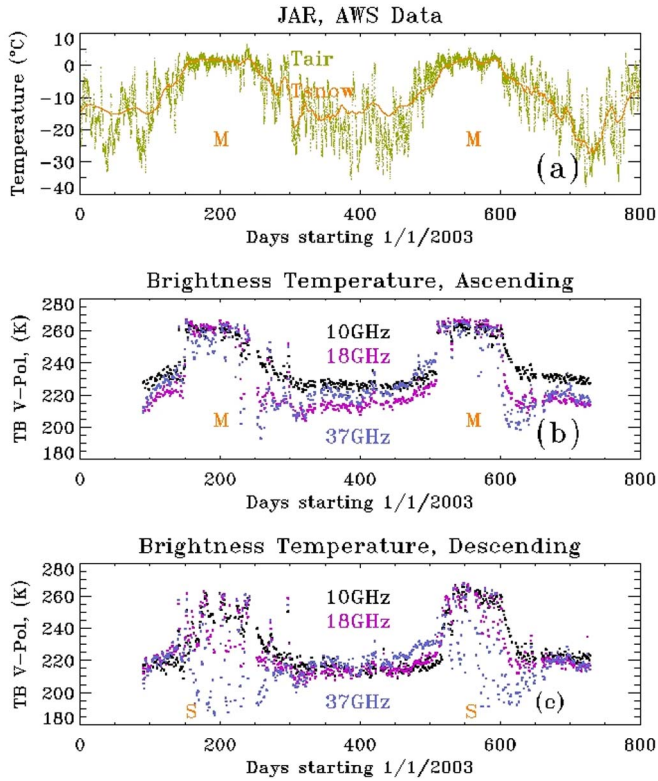

Fig. 8. Time series of WindSat observations over the JAR study site on Greenland from April 1, 2003 to December 30, 2004. The 10.7-, 18.7-, and 37.0-GHz data are color coded with black, purple, and blue, respectively. (a) *In situ* air and snow temperature. (b) Vertically polarized brightness temperature of ascending orbits. (c) Vertically polarized brightness temperature of descending orbits. The symbol "M" indicates melting period, and "S" suggests strong volume scattering.

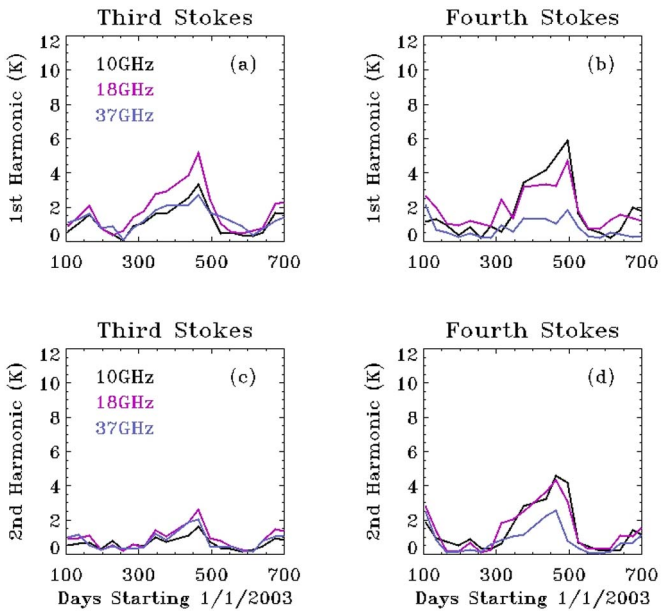

Fig. 9. Time series of WindSat observations over the JAR study site on Greenland from April 1, 2003 to December 30, 2004. The 10.7-, 18.7-, and 37.0-GHz data are color coded with black, purple, and blue, respectively. (a) First harmonic of U. (b) First harmonic of V. (c) Second harmonic of U. (d) Second harmonic of V.

of these two sites are different for the second harmonic of V [Figs. 5(d) and 7(d)]. The similarity in polarimetric signatures, and their seasonal variation, between these two sites confirms the repeatability of WindSat measurements. On the other hand, the observed differences in the polarimetric signatures provide opportunities to study snowpack structures.

C. Temporal Variations of Wet-Snow Zone

Microwave emission is very sensitive to snow wetness, and microwave radiometer data have been used to detect snowmelt over Greenland [1], [6], [7], [27]. For dry snow, volume scattering dominates the emission signatures due to the relatively small extinction coefficient and large scattering albedo. However, with even a very small amount of liquid water present in the snowpack, the scattering albedo is dramatically reduced to a very small value, and the large change in dielectric properties limits the penetration depth to a few wavelengths beneath the surface. With the near absence of volume scattering in the snow medium, the snowpack approaches the nonscattering characteristics of a nearly blackbody radiator [41]. To examine melting signatures, we extracted a time-series of WindSat data near the JAR site (69.50 °N, 49.68 °W) in the wet-snow zone, which is only about 16 km away from well-studied Swiss Camp site (69.57 °N, 49.32 °W). Abdalati and Steffen [1] used this Swiss Camp site to develop an SSM/I snowmelt algorithm for Greenland, and it will be interesting to use the same site to analyze WindSat data. However, there is a significant data gap in 2003 and 2004 for the Swiss Camp site due to an AWS instrument malfunction. Because of this data gap, we opted to use the JAR site for our analysis. Fortunately, the data from the two sites are very close for air and snow temperature measurements. Fig. 8(a) plots time-series of air temperature at 1-m height and snow temperature at 1-m depth, and WindSat vertically polarized brightness temperatures for ascending and descending passes.

From June to September [day 150 to 250, as indicated by "M" for melting period in Fig. 8(a) and (b)], the air and snow temperatures are quite stable with a mean of about 272 K and a diurnal variation of about 5 K. In Fig. 8(b), for ascending passes (4:30 P.M. local time), the brightness temperatures of the three frequencies are all quite stable approaching 267 K and are essentially frequency independent, a feature of strong snowmelt signature. For the descending passes (7:30 A.M. local time), refreezing of the wet or saturated snowpack generates larger snow grains, dries the snow, and enables much deeper penetration. As a result, volume scattering dominates the signature, as indicated by the very large difference (up to 70 K) between 18.7- and 37-GHz channels near the label "S" in Fig. 8(c).

As was the case for the dry zone sites, the polarimetric signatures shown in Fig. 9(a)–(d) for the JAR site are significant and exhibit well-defined seasonal variations. Polarimetric signatures at all frequencies are very weak in the summer (day 150 to 250 and 500 to 600), and are the strongest in late March (around 450). This means that the polarimetric harmonics drop quickly and significantly to about 1 K or lower when melting starts, and slowly increase once refreezing begins. Volume scattering is strongest during the summer when refreezing occurs at night during descending passes [as indicated by the "S" in Fig. 8(c)]. However, the very strong volume scattering does not produce a very strong polarimetric signal, probably because the ice crystals generated through melt/freeze cycling do not exhibit a strong azimuthal variation.

In general, the overall polarimetric signal strength is weaker for this wet-snow site than the dry-snow sites and, as shown in Fig. 9(c), the U second harmonic amplitude is always small. Another interesting feature is that the 18.7- and 37-GHz Stokes parameters are reduced much more, relative to the dry snow sites, than 10.7 GHz. One possible cause is that the melting and refreezing cycle reduces asymmetric structures through recrystallization near the surface, coincident with the 18.7- and 37-GHz penetration depths. Such metamorphic changes do not have a directional preference, reducing the general asymmetry of the firn structure. However, at the greater penetration depths of 10.7-GHz radiation, this process has much less impact. Further coordinated field, laboratory, and modeling work are necessary to fully understand these features.

VI. Summary

The four parameters of the Stokes vector provide a full characterization of polarization. The first and second modified Stokes parameters (T_{V} and T_{H}) have broad science applications and are widely used in microwave radiometry. All previous passive microwave satellite sensors measured only the first two modified Stokes parameters. Tsang [39] showed theoretically that random media of asymmetry structures can produce large polarimetric microwave signatures of the third and fourth Stokes parameters through volume and surface scattering [22], [43]. Subsequent ocean experimental studies observed significant third Stokes parameter (up to $\sim$2.5 K), but the fourth Stokes parameter is much smaller [48]. WindSat, the first spaceborne polarimetric microwave radiometer, detected, for the first time, distinct and strong third and fourth Stokes parameter signals up to 15 K over the polar region. In addition, WindSat data contain fourth Stokes parameters that are larger than the third Stokes parameters, also for the first time in nature. The polarimetric signature exhibits distinct geophysical and observation geometry signatures, which are related to asymmetrical structures of polar ice sheets, including possibly the millimeter-scale snow crystals, meter-scale surface roughness, and up to kilometer-scale moulins and crevasses. The third and fourth Stokes parameters have well-defined large azimuthal modulations and significant seasonal variations, which reflects geophysical variations in snow microstructure, melting, and possibly snow surface roughness. We used a second-order data observation model to separate and quantify the azimuthal modulation and extract polarimetric signature variations due to geophysical changes. The model data fit the observations very well. The extracted polarimetric signatures are relatively weak in the summer and are strongest near spring. This corresponds well with the formation and erosion of the sastrugi in the dry snow zone and snowmelt in the soaked zone. It is possible that the WindSat U and V data respond to the coupled volume and surface scattering associated with asymmetry structures of polar firn microstructure and rough surfaces.

Remote sensing data have long been used to study the roughness surface scattering by the asymmetry structure of sastrugi. For example, Ledroit *et al.* [21] attributed the azimuthal modulation of normalized radar cross-sectional measurements to sastrugi and correlated such a modulation with the katabatic wind direction. Ashcraft and Long [8] assume that snow surface

roughness at the 3–300-m scales are the primary mechanism driving the modulation, and developed successfully an ERS scatterometer model to extract the azimuthal modulation and surface snow properties. When compared with normalized radar cross-sectional data, the WindSat third and fourth Stokes parameters are the only satellite measurements that respond primarily to the asymmetry structures of polar snow and show very clean azimuthal modulations. In addition, the fourth Stokes parameter responds solely to the snow microstructure at the centimeter wavelength scales and can be used to separate snow large- and small-scale structures. In the subsequent research, we will explore similar applications for WindSat and compare the active scatterometer and passive radiometer results. Similarly, in the optical band, Warren *et al.* [44] examined the angular pattern of sunlight reflection by snow surface and demonstrated the significant impacts by oriented sastrugi for large incidence angles. Nolin *et al.* [28] take advantage of the MISR multiangular data and defined a normalized difference angular index which is correlated with surface roughness on the scale of 70 m. A future comparison of MISR surface roughness maps [29] with WindSat data, both spatially and temporally, can help us to understand the impact of surface roughness on polarimetric signals.

ACKNOWLEDGMENT

The authors would like to thank Dr. K. Steffen of the University of Colorado at Boulder for providing GC-Net data. The authors would also like to thank Dr. R. Bevilacqua of NRL and Dr. K. Steffen for valuable discussions and information.

REFERENCES

[1] W. Abdalati and K. Steffen, "Snowmelt on the Greenland ice sheet as derived from passive microwave satellite data," *J. Clim.*, vol. 10, no. 2, pp. 165–175, Feb. 1997.

[2] W. Abdalati and K. Steffen, "Accumulation and hoar effects on microwave emission on the Greenland ice-sheet dry-snow zones," *J. Glaciol.*, vol. 44, no. 148, pp. 523–531, 1998.

[3] M. R. Albert and R. Hawley, "Seasonal changes in snow surface roughness characteristics at Summit, Greenland: Implications for snow and firn ventilation," *Ann. Glaciol.*, vol. 35, no. 1, pp. 510–514, Jan. 2002.

[4] R. B. Alley, *The Two-Mile Time Machine*. Princeton, NJ: Princeton Univ. Press, 2000.

[5] I. S. Ashcraft and D. G. Long, "Observation and characterization of radar backscatter over Greenland," *IEEE Trans. Geosci. Remote Sens.*, vol. 43, no. 2, pp. 225–237, Feb. 2005.

[6] I. S. Ashcraft and D. G. Long, "Comparison of methods for melt detection over Greenland using active and passive microwave measurements," *Int. J. Remote Sens.*, vol. 27, no. 12, pp. 2469–2488, Jun. 2006.

[7] I. S. Ashcraft and D. G. Long, "Differentiation between melt and freeze stages of the melt cycle using SSM/I channel ratios," *IEEE Trans. Geosci. Remote Sens.*, vol. 43, no. 6, pp. 1317–1323, Jun. 2005.

[8] I. S. Ashcraft and D. G. Long, "Relating microwave backscatter azimuth modulation to surface properties of the Greenland ice sheet," *J. Glaciol.*, vol. 52, no. 177, pp. 257–266, Mar. 2006.

[9] M. H. Bettenhausen, C. K. Smith, R. M. Bevilacqua, N. Wang, P. W. Gaiser, and S. Cox, "A nonlinear optimization algorithm for WindSat wind vector retrievals," *IEEE Trans. Geosci. Remote Sens.*, vol. 44, no. 3, pp. 597–610, Mar. 2006.

[10] C. S. Benson, "Stratigraphic studies in the snow and firn of the Greenland ice sheet," U.S. Army Cold Regions Res. Eng. Lab., Hanover, NH, SIPRE Res. Rep. 70, 1962.

[11] F. Domine and P. L. Shepson, "Air-snow interactions and atmospheric chemistry," *Science*, vol. 297, no. 5586, pp. 1506–1510, Aug. 2002.

[12] J. D. Flach, K. C. Partington, C. Ruiz, E. Jeansu, and M. R. Drinkwater, "Inversion of the surface properties of ice sheets from satellite microwave data," *IEEE Trans. Geosci. Remote Sens.*, vol. 43, pp. 743–752, 2005.

[13] A. K. Fung and M. F. Chen, "Emission from an inhomogeneous layer with irregular interfaces," *Radio Sci.*, vol. 16, no. 3, pp. 289–298, 1981.

[14] P. W. Gaiser, K. M. St. Germain, E. M. Twarog, G. A. Poe, W. Purdy, D. Richardson, W. Grossman, W. L. Jones, D. Spencer, G. Golba, J. Cleveland, L. Choy, R. M. Bevilacqua, and P. Chang, "The WindSat spaceborne polarimetric microwave radiometer: Sensor description and early orbit performance," *IEEE Trans. Geosci. Remote Sens.*, vol. 42, no. 11, pp. 2347–2361, Nov. 2004.

[15] K. M. G. Germain, G. A. Poe, and P. W. Gaiser, "Polarimetric emission model of the sea at microwave frequencies and comparison with measurements," *Prog. Electromagn. Res.*, vol. 37, pp. 1–30, 2002.

[16] A. J. Gow, "Snow studies in Antarctica," U.S. Army Cold Regions Res. Eng. Lab., Hanover, NH, CRREL Rep. RR 177, 1965.

[17] A. J. Gow and R. Rowland, "On the relationship of snow accumulation to surface topography at 'Byrd Station,' Antartica," *J. Glaciol.*, vol. 5, no. 42, pp. 843–847, 1965.

[18] N. C. Grody and A. N. Basist, "Interpretation of SSM/I measurements over Greenland," *IEEE Trans. Geosci. Remote Sens.*, vol. 35, no. 2, pp. 360–366, Mar. 1997.

[19] D. K. Hall, A. T. C. Chang, and J. L. Foster, "Detection of the depth-hoar layer in the snow-pack of the Arctic Coastal Plain of Alaska, U.S.A., using satellite data," *J. Glaciol.*, vol. 32, no. 110, pp. 87–94, 1986.

[20] U. C. Herzfeld, "Geostatistical interpolation and classification of remote sensing data from ice surfaces," *Int. J. Remote Sens.*, vol. 20, no. 2, pp. 307–327, Jan. 1999.

[21] M. Ledroit, F. Remy, and J. F. Minster, "Observation of the Antarctica ice sheet by seasat scatterometer: Relation to Katabatic wind intensity and direction," *J. Glaciol.*, vol. 39, no. 132, pp. 383–396, 1993.

[22] L. Li, C. H. Chan, and L. Tsang, "Numerical simulation of conical diffraction of tapered electromagnetic waves from random rough surfaces and applications to passive remote sensing," *Radio Sci.*, vol. 29, no. 3, pp. 587–598, 1994.

[23] D. G. Long and M. R. Drinkwater, "Greenland ice-sheet surface properties observed by the Seasat—A scatterometer at enhanced resolution," *J. Glaciol.*, vol. 40, no. 135, pp. 213–230, 1994.

[24] D. G. Long and M. R. Drinkwater, "Azimuth variation in microwave scatterometer and radiometer data over Antarctica," *IEEE Trans. Geosci. Remote Sens.*, vol. 38, no. 4, pp. 1857–1870, Jul. 2000.

[25] C. Mätzler, "Applications of the interaction of microwaves with natural snow cover," *Remote Sens. Rev.*, vol. 2, pp. 259–387, 1987.

[26] C. Mätzler, "Passive microwave signatures of landscapes in winter," *Meteorol. Atmos. Phys.*, vol. 54, no. 1–4, pp. 241–260, Mar. 1994.

[27] T. L. Mote and M. R. Anderson, "Variations in snowpack melt on the Greenland ice sheet based on passive-microwave measurements," *J. Glaciol.*, vol. 41, no. 137, pp. 51–60, 1995.

[28] A. W. Nolin, F. M. Fetterer, and T. A. Scambos, "Surface roughness characterizations of sea ice and ice sheets: Case studies with MISR data," *IEEE Trans. Geosci. Remote Sens.*, vol. 40, no. 7, pp. 1605–1615, Jul. 2002.

[29] A. W. Nolin and M. C. Payne, "Classification of glacier zones in western Greenland using albedo and surface roughness from the Multi-angle Imaging SpectroRadiometer (MISR)," *Remote Sens. Environ.*, vol. 107, no. 1/2, pp. 264–275, Mar. 2007.

[30] J. R. Piepmeier and A. J. Gasiewski, "High-resolution passive polarimetric microwave mapping of ocean surface wind vector fields," *IEEE Trans. Geosci. Remote Sens.*, vol. 39, no. 3, pp. 606–622, Mar. 2001.

[31] C. A. Shuman, R. B Alley, and S. Anandakrishnan, "Characterization of a hoar-development episode using SSM/I brightness temperatures in the vicinity of the GISP2 site, Greenland," *Ann. Glaciol.*, vol. 17, pp. 183–188, 1993.

[32] C. A. Shuman, R. B Alley, S. Anandakrishnan, and D. R. Stearns, "An empirical technique for estimating near-surface air temperature trends in central Greenland from SSM/I brightness temperatures," *Remote Sens. Environ.*, vol. 51, no. 2, pp. 245–252, Feb. 1995.

[33] K. Steffen, J. E. Box, and W. Abdalati, "Greenland climate network: GC-Net," in "Glaciers, Ice Sheets, and Volcanoes: A Tribute to Mark F. Meier," U.S. Army Cold Regions Res. Eng. Lab., Hanover, NH, pp. 98–103, CRREL Special Rep. 96-27, 1996.

[34] K. Steffen, W. Abdalati, and I. Sherjal, "Faceted crystal formation in the northeast Greenland low-accumulation region," *Ann. Glaciol.*, vol. 45, no. 149, pp. 63–68, 1999.

[35] M. Sturm and C. Benson, "Scales of spatial heterogeneity for perennial and seasonal snow layers," *Ann. Glaciol.*, vol. 38, no. 1, pp. 253–260, Jan. 2004.

[36] S. Surdyk and M. Fily, "Results of a stratified snow emissivity model based on the wave approach: Application to the Antarctic ice sheet," *J. Geophys. Res.*, vol. 100, no. C5, pp. 8837–8848, 1995.

[37] S. Surdyk, "Using microwave brightness temperature to detect short-term surface air temperature changes in Antarctica: An analytical approach," *Remote Sens. Environ.*, vol. 80, no. 2, pp. 256–271, May 2002.

[38] L. Tsang, J. A. Kong, and R. T. Shin, *Theory of Microwave Remote Sensing*. New York: Wiley, 1985.
[39] L. Tsang, "Polarimetric passive microwave remote sensing of random discrete scatterers and rough surfaces," *J. Electromagn. Waves Appl.*, vol. 5, no. 1, pp. 41–57, 1991.
[40] F. Ulaby, R. Moore, and A. K. Fung, *Microwave Remote Sensing: Active and Passive*, vol. 1. Norwood, MA: Artech House, 1981.
[41] F. Ulaby, R. Moore, and A. K. Fung, *Microwave Remote Sensing: Active and Passive*, vol. 3. Norwood, MA: Artech House, 1986.
[42] C. J. Van der Veen and K. C. Jezek, "Seasonal variations in brightness temperature for central Antarctica," *Ann. Glaciol.*, vol. 17, pp. 300–306, 1993.
[43] M. E. Veysoglu, H. A. Yueh, R. T. Shin, and J. A. Kong, "Polarimetric passive remote sensing of periodic surfaces," *J. Electromagn. Waves Appl.*, vol. 5, no. 3, pp. 267–280, 1991.
[44] S. G. Warren, R. E. Brandt, and P. O. Hinton, "Effect of surface roughness on bidirectional reflectance of Antarctic snow," *J. Geophys. Res.*, vol. 103, no. E11, pp. 25 789–25 807, 1998.
[45] R. West, D. P. Winebrenner, L. Tsang, and H. Rott, "Microwave emission from density-stratified Antarctic firn at 6 cm wavelength," *J. Glaciol.*, vol. 42, no. 140, pp. 63–76, 1996.
[46] P. Xu, L. Tsang, L. Li, and K. S. Chen, "Emissivities of rough surface over layered media in microwave remote sensing of snow," in *Proc. Int. Geosci. Remote Sens. Symp.*, Barcelona, Spain, 1996, pp. 1436–1439.
[47] S. H. Yueh, R. Kwok, F. K. Li, S. V. Nghiem, W. J. Wilson, and J. A. Kong, "Polarimetric passive remote sensing of ocean wind vectors," *Radio Sci.*, vol. 29, no. 4, pp. 799–814, 1994.
[48] S. H. Yueh, W. J. Wilson, F. K. Li, S. V. Nghiem, and W. B. Ricketts, "Polarimetric measurements of sea surface brightness temperatures using an aircraft K-band radiometer," *IEEE Trans. Geosci. Remote Sens.*, vol. 33, no. 1, pp. 85–92, Jan. 1995.
[49] S. H. Yueh, "Modeling of wind direction signals in polarimetric sea surface brightness temperatures," *IEEE Trans. Geosci. Remote Sens.*, vol. 35, no. 6, pp. 1400–1418, Nov. 1997.
[50] H. J. Zwally, "Microwave emissivity and accumulation rate of polar firn," *J. Glaciol.*, vol. 18, no. 79, pp. 195–215, 1977.

Li Li (M'96–SM'06) received the M.S. degree in electrical engineering from the Beijing University of Posts and Telecommunications, Beijing, China, in 1987 and the Ph.D. degree in electrical engineering from the University of Washington, Seattle, in 1995.

He is currently with the Naval Research Laboratory, Washington, DC, working on spaceborne radiometry of land and ocean, particularly the algorithm study for the WindSat spaceborne radiometer and risk reduction for the National Polar-orbiting Operational Environmental Satellite System (NPOESS) Microwave Imager/Sounder. From 1997 to 2004, he was a Senior Scientist with the Jet Propulsion Laboratory (JPL), California Institute of Technology, Pasadena. He was a Visiting Student from 1993 to 1995 at the National Center for Atmospheric Research, Boulder, CO. From 1995 to 1997, he was with the Caelum Research Corporation, working at the National Oceanic and Atmospheric Administration/National Environmental Satellite, Data, and Information Service Office of Research and Application, Camp Springs, MD.

Dr. Li is a member of the American Geophysical Union. He was the recipient of the 1993–1995 National Center for Atmospheric Research/Research Applications Program Fellowship. He received the National Aeronautics and Space Administration Group Achievement Awards in 2002 and the JPL Technical Excellence Award in 2002.

Peter Gaiser (S'91–M'93–SM'04) received the B.S. degree in electrical engineering from the Virginia Polytechnic Institute and State University, Blacksburg, in 1987 and the Ph.D. degree from the University of Massachusetts, Amherst, in 1993, where he studied microwave remote sensing, with emphasis on synthetic aperture interferometric radiometry.

He has been with the Naval Research Laboratory (NRL), Washington, DC, since 1993, and is currently the Head of the Remote Sensing Physics Branch, Remote Sensing Division. While at NRL, he has been involved in a variety of microwave and millimeter-wave radiometry projects, with concentration on polarimetric radiometry research. His research interests include instrument design, development, and calibration, data collection, and model development specifically for the purpose of ocean wind vector measurements from space. He is the Principal Investigator for the WindSat spaceborne polarimetric microwave radiometer demonstration project.

Mary R. Albert received the B.S. degree in mathematics from Pennsylvania State University, University Park, in 1975, the B.E. and M.S. degrees in engineering sciences from Dartmouth College, Hanover, NH, in 1983, and the Ph.D. degree in engineering sciences from the University of California, San Diego, in 1991.

She is a Senior Research Engineer with the Army Cold Regions Research and Engineering Laboratory, Hanover, NH, where her research is centered on transfer processes in porous media, including air-snow exchange in the polar regions and in soils in temperate areas. She is also an Adjunct Professor of engineering with the Thayer School of Engineering, Dartmouth College, where she serves as a Thesis Advisor to students at the undergraduate, master's, and Ph.D. levels. She has been the Principal Investigator on many research projects in Greenland and Antarctica. She currently serves on the Government Performance and Results Act Advisory Committee for the National Science Foundation, the Executive Committee of the American Geophysical Union Cryosphere Focus Group, the Editorial Boards of *Hydrological Processes* and *Cold Regions Science and Technology*, and, in the past, has served on the National Research Council Polar Research Board.

Dr. Albert was the recipient of the 1989 Department of the Army Research and Development Award and the 1996 U.S. Army Corps of Engineers Women in Science Achievement Award. She has received numerous Equal Employment Opportunity and Special Act Awards.

David G. Long (S'80–F'08) received the Ph.D. degree in electrical engineering from the University of Southern California, Los Angeles, in 1989.

From 1983 to 1990, he was with NASA's Jet Propulsion Laboratories (JPL), where he developed advanced radar remote sensing systems. While with JPL, he was the Project Engineer on the NASA Scatterometer (NSCAT) project, which flew from 1996 to 1997. He also managed the SCANSCAT project, the precursor to SeaWinds, which was launched in 1999 and 2002. He is currently a Professor with the Electrical and Computer Engineering Department, Brigham Young University (BYU), where he teaches upper division and graduate courses in communications, microwave remote sensing, radar, and signal processing and is the Director of the BYU Center for Remote Sensing. He is the Principle Investigator on several NASA-sponsored research projects in remote sensing. He has numerous publications in signal processing and radar scatterometry. His research interests include microwave remote sensing, radar theory, space-based sensing, estimation theory, signal processing, and mesoscale atmospheric dynamics. He has nearly 300 publications.

Dr. Long has received the NASA Certificate of Recognition several times. He is an Associate Editor for the IEEE GEOSCIENCE AND REMOTE SENSING LETTERS.

Elizabeth M. Twarog received the B.S. degree from the University of Massachusetts, Amherst, and the M.S. and Ph.D. degrees from Northeastern University, Boston, MA, in 1992, 1995, and 1998, respectively, all in electrical engineering.

From 1993 to 1998, she was with the Radar Systems Laboratory in the field of polarimetric low grazing angle radar sea scatter and airborne radar imaging of the coastal ocean. Since joining the Passive Microwave Section, Remote Sensing Division, Naval Research Laboratory, Washington, DC, in 1999, she has been involved with microwave spaceborne polarimetric radiometry. She was a member of the WindSat satellite technical and science teams. Her research interests include microwave receiver system testing, satellite postlaunch calibration, and passive millimeter-wave interferometry.